Heavy flavour hadron production in relativistic heavy ion collisions at RHIC and LHC in EPOS4HQ

Jiaxing Zhao, ¹ Joerg Aichelin, ¹ Pol Bernard Gossiaux, ¹ Vitalii Ozvenchuk, ² and Klaus Werner ¹ SUBATECH, Nantes University, IMT Atlantique, IN2P3/CNRS, ⁴ rue Alfred Kastler, 44307 Nantes cedex 3, France ² Institute of Nuclear Physics, Polish Academy of Sciences, Cracow, Poland (Dated: February 28, 2024)

Employing the recently developed EPOS4HQ event generator, we study the production of different heavy-flavor mesons in relativistic heavy-ion collisions at RHIC and LHC energies. The transverse momentum spectra, yield ratio, nuclear modification factor, and elliptic flow can be well described in the EPOS4HQ framework. We furthermore analyze the processes which modify these observables as compared to pp collisions and are at the origin of the experimentally determined nuclear modification factor R_{AA} .

I. INTRODUCTION

Theory predicts that matter at high temperature and/or high density forms a plasma of quarks and gluons (QGP) in which partons are not confined anymore. One of the main goals of heavy-ion reactions at ultrarelativistic energies is to study this new form of deconfined matter. In the last years ample evidence has been gathered that this state exists. The observation of strangeness enhancement [1], flow harmonics compatible with hadronization after an hydrodynamic expansions [2], jet quenching [3], and quarkonium suppression [4] points in this direction.

Presently the main objective is to get a more quantitative understanding and investigate the properties of the QGP matter.

The agreement of observables like spectra and flow harmonics with viscous hydrodynamical calculations reveals the strongly-coupled nature of the QGP. The very small viscosity η/s [5], which is necessary to bring the calculations in agreement with data, is close to the lowest possible limit given by AdS/CFT [6]. So we have strong evidence that a system has been created that behaves as an almost ideal fluid.

Despite the fact that we have a good qualitative understanding about the space-time evolution of the system, there are many open questions when it comes to a quantitative analysis. The above-mentioned probes (yields, spectra, flow harmonics) give only an indirect access to the properties of expanding system, one has to rely on model calculations or simulations - which have uncertainties. So we need additional probes to get complementary information about the system, done in the same model / simulation. Heavy flavor hadrons have turned out to be an almost ideal probe to study the time evolution of the QGP due to the following reasons: a) The heavy quark mass ($m_c = 1.5 \text{GeV}$ and $m_b = 4.5 \text{GeV}$) is much larger than the QCD cutoff, $\Lambda_{QCD} \approx 200 \mathrm{MeV}$. Therefore their production can be well described by perturbative QCD (pQCD). b) Heavy quarks are produced at the early stage of a heavy ion collisions and witness all later stages of the collision; c) The heavy quark mass is much larger than

the typical temperature of the QGP medium, which is about a couple of hundreds of MeV, estimated by the spectrum of the directly produced photons [7]. Consequently, the mass of heavy quark changes little in the hot medium and their number is conserved during the evolution.

With these advantages, heavy flavor physics has attracted a lot of attention from both the theoretical and experimental communities and several models have been advanced to describe the heavy flavor observables. The PHSD [8, 9] approach, in which the heavy quark physics is embedded in an approach which described the light hadrons as well, is based in the dynamical quasi particle model (DQPM), which respects the equation of state of strongly interacting matter. The Catania model [10–12] is also based on a DQPM approach and describes the expanding medium by a Boltzmann equation. Based on the EPOS3 event generator we have also studied heavy quark production [13] using a elastic and inelastic pQCD cross sections. The LBT model [14] solves as well a Boltzmann equation for the heavy quarks including elastic and inelastic collisions but the medium is described by viscous hydrodynamics. Other models like TAMU[15, 16], Duke [17] and Torino [18, 19] use a Fokker Planck equation to describe the dynamics of heavy quarks and model model the expanding QGP by ideal or viscous hydrodynamics. Apart from PHSD and EPOS all these models have in common that they concentrate on heavy quark physics only and do not take advantage of the fact that the many light hadron observables allow for assessing the expansion of the QGP despite different expansion properties of the QGP may have a strong influence on the heavy quark observables [20].

Thanks to the high statistic data, which are now or become soon available, the error of the key observables, such as the enhancement of the baryon to meson ratio and the elliptic flow, are strongly reduced. This allows for a detailed quantitative comparison between theory and experiment. In this paper we compare the heavy hadron observables with the results of EPOS4HQ. EPOS4HQ is the heavy hadron extension of the recently advanced EPOS4 approach [21–24], which has been suc-

cessfully used to study the light hadron observables. In the EPOS4HQ approach the heavy flavor production has been substantially improved in comparison with the former EPOSLHC approach. Heavy flavor quarks can now be produced in hard process, as well as by gluon splitting and flavour excitation. The interaction of heavy partons with the QGP includes elastic and gluon emission reactions refs. [25, 26]. After the hadronization the heavy hadrons still have final state interactions, modeled by UrQMD. The calculations are based on version EPOS4.0.1.s9.

In this paper we will systematically investigate all published heavy favor observables. It is organized as follows. The heavy quark initial production and the medium evolution in EPOS4HQ are discussed in Section II. Next, the heavy quark initial spectra and energy loss mechanism is subject of Sections III and IV. In Section V, we will present the hadronization in EPOS4HQ, which differs substantially from former heavy quark calculations with EPOS2/EPOS3/EPOSLHC by including baryons and excited mesons states. The results and the comparison with experimental data are shown in Section VI. A conclusion will be given in Section VII.

II. EPOS4

A. EPOS4 primary interactions

A fundamental ingredient of the EPOS4 approach [21–24] is the observation that multiple partonic scatterings must strictly happen in parallel, and not sequentially, based on very elementary considerations concerning time-scales. To take this into account, EPOS4 brings together ancient knowledge about S-matrix theory (to deal with parallel scatterings) and modern concepts of perturbative QCD and saturation, going much beyond the usual factorization approach. The parallel scattering principle requires sophisticated Monte Carlo techniques, inspired by those used in statistical physics to investigate the Ising model.

In the EPOS4 approach, we distinguish "primary scatterings" and "secondary scatterings". The former refer to the above-mentioned parallel scatterings with the initial nucleons (and their partonic constituents) being involved, happening at very high energies instantaneously. The theoretical tool is S-matrix theory, using a particular form of the proton-proton scattering S-matrix ("classical" Gribov-Regge approach [27–30]). Within such an approach, one can deduce the very important AGK theorem [30], which leads to factorization and binary scaling in nuclear scatterings, which is not trivial in a multiple scattering scheme. However, introducing energy-momentum sharing [31] (which is absolutely crucial for realistic event-by-event simulations, AGK is violated (and so is factorization and binary scaling). The main new development in EPOS4 [21–24] is a way to accomodate simultaneously: (1) rigorous parallel scattering, (2) energy-momentum sharing, (3) AGK theorem and factorization for hard processes, by introducing (in a very particular way) saturation, compatible with recent "low-x-physics" considerations [32–43].

Validity of AGK means that we can do the same as models based on factorization (defining nand using parton distribution fuctions) to study very hard processes, but this represents only a very small fraction of all possible applications, and there are very interesting cases outside the applicability of that approach. A prominent example, one of the highlights of the past decade in our domain, concerns collective phenomena in small systems. It has been shown that high-multiplicity pp events show very similar collective features as earlier observed in heavy ion collisions [44]. High multiplicity means automatically "multiple parton scattering". As discussed earlier, this means that we have to employ the full parallel scattering machinery developed earlier, based on Smatrix theory. We cannot use the usual parton distribution functions (representing the partonic structure of a fast nucleon), we have to treat the different scatterings (happening in parallel) individually, for each one we have a parton evolution according to some evolution function E (representing the partonic structure of a fast parton), as sketched in Fig. 1. We still have DGLAP evolution,

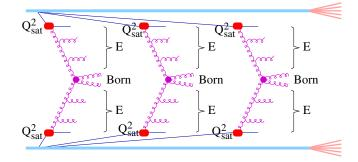


FIG. 1. Rigorous parallel scattering scenario, for n=3 parallel scatterings, including non-linear effects via saturation scales. The red symbols should remind us that the parts of the diagram representing nonlinear effects are replaced by simply using saturation scales.

for each of the scatterings (we only show the spacelike (SL) cascade), but we introduce saturation scales. But, most importantly, these scales are not constants, they depend on the number of scatterings, and they depend as well on x^+ and x^- . An example of a multiple scattering AA configuration is shown in Fig. 2.

B. EPOS4 heavy quark issues

At each step in the SL cascade, there is the possibility of quark-antiquark production, and in the Born process as well. In the following, we discuss in particular the case of heavy flavor quarks, with the general notation Q for quarks and \bar{Q} for antiquarks (for details see Ref.

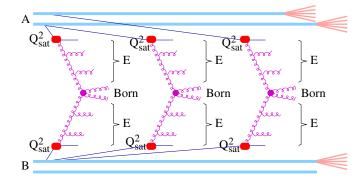


FIG. 2. Rigorous parallel scattering scenario, for n=3 parallel scatterings for a collision of a nucleus A with a nucleus B, including non-linear effects via saturation scales.

[22]). Heavy flavor may be produced in different ways, as shown in Fig. 3. Starting from a gluon, a $Q - \bar{Q}$

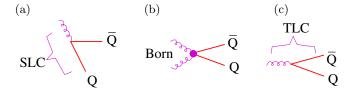


FIG. 3. Different possibilities to create heavy flavor, (a) in the space-like cascade (SLC), (b) in the Born process, (c) in the time-like cascade (TLC).

pair may be produced in the SL cascade, as shown in Fig. 3(a), provided the virtuality is large enough. The number of allowed flavors is considered to be depending on the virtuality (variable flavor number scheme). It is also possible to create a $Q - \bar{Q}$ in the Born process, via $g + g \rightarrow Q + \bar{Q}$ or $q + \bar{q} \rightarrow Q + \bar{Q}$ (for light flavor quarks q), as shown in Fig. 3(b), and finally $Q - \bar{Q}$ may be produced in the TL cascade, via $g \to Q + \bar{Q}$, as shown in Fig. 3(c). Let us first consider the $Q - \bar{Q}$ production in the SLC. We may have the situation as shown in Fig. 4(a), where a heavy flavor parton (here a \bar{Q}) is emitted, and the corresponding antiparticle (here a Q) continues the SLC. But before reaching the Born process, it is emitted, and a gluon continues the SLC. The two heavy flavor partons have in general low transverse momenta. Another possibility is shown in Fig. 4(b), where a heavy flavor parton produced in the SLC "survives" till the Born process, and the latter has most likely the form $Q+l \rightarrow Q+l$, with l being a light flavor parton. Other than the production during the SLC, heavy flavor may be produced in the Born process, via $g+g \to Q + \bar{Q}$ or $q+\bar{q} \to Q + \bar{Q}$ (for light flavor quarks q), as shown in Fig. 4(c). Finally, heavy flavor may be produced during the time-like cascade, as shown in Fig. 5, either initiated from a TL parton in the SL cascade (Fig. 5(a)), or initiated from an outgoing parton of the Born process (Fig. 5(b)). In the first case, the transverse momenta are in general small.

The next step will be, for a given Feynman diagram, to

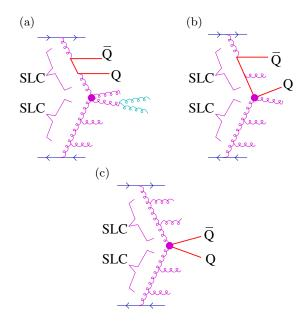


FIG. 4. Heavy flavor production (a,b) in the SL cascade and (c) in the Born process. The magenta point indicated the Born process.

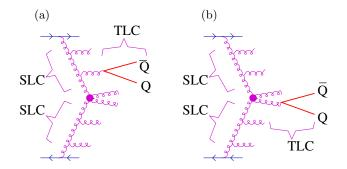


FIG. 5. Heavy flavor production in the TL cascade.

construct the color flow diagram. Let us take the graph of Fig. 5(b), i.e. heavy flavor production during the TLC of an outgoing Born parton. As usual, the gluons are emitted to either side with equal probability, so a possible color flow diagram is the one shown in Fig. 6. We identify three chains of partons: 1-2-3-4-5, 6-7-8, and 9-10-11. The initial TL partons (the horizontal blue lines with arrows) or most likely quarks and antiquarks (in any case 3 and $\bar{3}$ color representations). Let us assume that 3 is a quark, and 6 an antiquark (light flavor, both), then the two chains containing heavy flavor are of the form $\bar{Q}-g-q$ and $\bar{q}-g-Q$, in both cases, the heavy flavor partons are "end partons" in the chains.

These chains of partons are finally mapped (in a unique fashion) to kinky strings, where each parton corresponds to a kink, as shown in Fig. 7. The general mapping procedure (chains of partons to kinky strings) as well as the string decay procedures (producing so-called "prehadrons") are described in detail in [31].

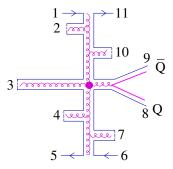


FIG. 6. A possible color flow diagram corresponding to the graph of Fig. 5(b)

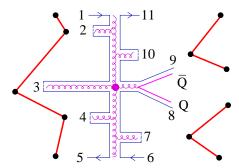


FIG. 7. The chains 1-2-3-4-5, 6-7-8, and 9-10-11 are mapped to kinky strings (red lines). The black points indicate the kinks, which carry the parton momenta.

C. EPOS4 core-corona method and fluid evolution

The above-mentioned parallel scattering happens at zero time. After that, we obtain a more or less important number of prehadrons. We employ a core-corona procedure [24, 45–47], where the prehadrons, considered at a given proper time τ_0 , are separated into "core" and "corona" prehadrons, depending on the energy loss of each prehadron when traversing the "matter" composed of all the others. Corona prehadrons (per definition) can escape, whereas core prehadrons lose all their energy and constitute what we call "core", which acts as an initial condition for a hydrodynamic evolution [47, 48]. The evolution of the core ends whenever the energy density falls below some critical value $\epsilon_{\rm FO}$, which marks the point where the fluid "decays" into hadrons. It is not a switch from fluid to particles, it is a sudden decay, called "hadronization". Let us consider a (randomly chosen, but typical) 5.02 ATeV lead-lead scattering. In Fig. 8, we plot the energy density in the transverse plane (x, y). We consider two snapshots, namely at the start time of the hydro evolution τ_0 (upper plot) and a later time τ_1 close to final freeze-out (lower plot). The initial distribution has an elongated shape (just by accident, due to the random positions of interacting partons). One can clearly see that the final distributions are as well elongated, but perpendicular to the initial ones, as expected

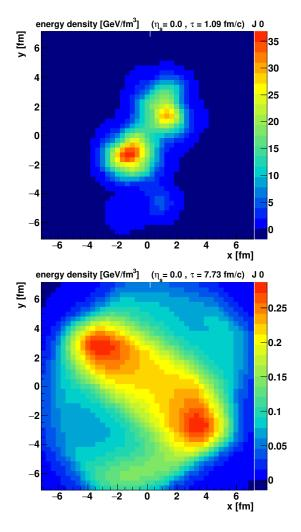


FIG. 8. Energy density in the transverse plane (x,y) for a Pb-Pb collision at $\sqrt{s_{\mathrm{NN}}} = 5.02$ TeV with an impact paremeter of 10.4 fm. The upper plot represents the start time τ_0 (of the hydro evolution), and the lower plot a later time τ_1 , close to final freeze-out.

in a hydrodynamical expansion. More examples can be found in [24].

In EPOS4, as discussed in detail in [24], we developed a new procedure of energy-momentum flow through the "freeze-out (FO) hypersurface" defined by $\epsilon_{\rm FO}$, which allows defining an effective invariant mass, decaying according to microcanonical phase space into hadrons, which are then Lorentz boosted according to the flow velocities computed at the FO hypersurface. We also developed new and very efficient methods for the microcanonical procedure [24]. Also in the full scheme, including primary and secondary interactions, energy-momentum and flavors are conserved.

III. INITIAL CHARM QUARK MOMENTUM DISTRIBUTION

EPOS2 and EPOS3 provided only the interaction points at which charm and anticharm quarks have been produced. Their transverse momentum had been chosen to reproduce the FONLL calculations [49, 50] and energy and momentum has not been conserved at the interaction points. Correlations between the heavy quark and antiquark have not been considered.

EPOS4, on the contrary, provides the correlation between the momenta of the charm and the anticharm quark, which are created at the same vertex. These correlations are difficult to compare with other approaches. Only PYTHIA provides this correlation as well. In the standard version of PYTHIA, however, only the leading order cross section is calculated and therefore the opening angle between c and \bar{c} is 180°. Including initial and final state interaction this distribution is modified but a one to one correspondence with the diagrams included in EPOS4 is not possible. The initial single (anti)charm quark p_T distribution, given by EPOS4HQ for pp collision can be compared with the fixed order next to leading log (FONLL) calculations [49, 50], the most advanced pQCD approach for describing single charm quark distributions. In Fig. 9 we display the FONLL and EPOS4 single charm and bottom quark distribution for 5.02 TeV pp collisions. We see that the EPOS4 distribution is at the upper limit of the error bars of the FONLL calculation for low p_T and consistent with FONLL for high p_T . This means that EPOS4 gives a larger charm production cross section, which is consistent with the experimental data obtained recently [51]. When produced in heavy-ion collisions, shadowing, saturation effects and the Cronin effect modify the initial (anti)charm quark distribution. In Fig. 10 we compare for PbPb at $\sqrt{s_{\rm NN}} = 5.02$ TeV the extrapolated pp p_T distribution (black dashed line) with the PbPb p_T distribution, which takes the above mention cold nuclear matter effects into account (blue line). At large p_T both distribution are almost identical but at low p_T one sees differences.

IV. EPOS4HQ: HEAVY QUARK ENERGY LOSS IN HOT MEDIUM

In contradistinction to EPOS4, in EPOS4HQ heavy quarks interact with the partons of the QGP, formed by the light partons and gluons from the core. We include in this study both, elastic [25] and radiative [26] collisions. To determine where the interaction takes place, we calculate the interaction rate and move the heavy quark to the interaction point, select whether the QGP parton is a gluon or a quark and draw the momentum of the scattering QGP parton from its corresponding thermal distribution. The thermal distribution is determined by the local temperature and mean velocity at the position at which the collision takes place. The scattering cross

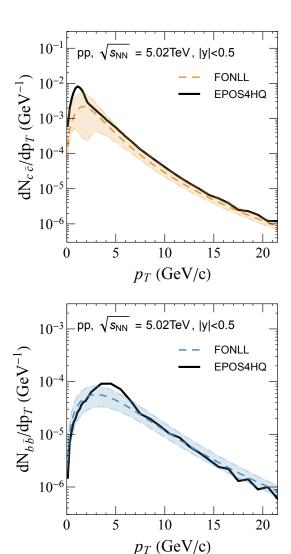


FIG. 9. The initial transverse momentum distribution of charm (upper) and bottom (lower) quarks for pp collisions at 5.02TeV. The solid black line is the EPOS4HQ calculation, while the orange (blue) dashed line presents the FONLL [49] result. The uncertainty of the FONLL result is given by the orange (blue) shaded area.

sections of the heavy quark with gluons and light quarks are calculated by pQCD matrix elements with a running coupling constant.

The pQCD elastic scattering cross section diverges for a small momentum transfer in the t and u channels. These infrared divergences are healed by the Debye screening mass $m_D(T)$ of gluons in the hot medium, which is calculated in the hard thermal loop (HTL) approach. It serves as a regulator of the propagator of the exchanged gluon. Scattering at high momentum transfer is, on the contrary, described by a free gluon propagator for massless gluons. A smooth transition of the energy loss between both regimes can be assured by an effective Debye mass $m_{\rm eff} = \kappa m_D(T)$ in the gluon propagator,

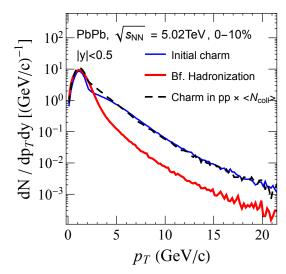


FIG. 10. The transverse momentum distribution of charm quarks at creation and before hadronization for central PbPb collisions at $\sqrt{s_{\rm NN}}=5.02~{\rm TeV}$. The transverse momentum distribution observed in pp collisions, multiplied by the number of initial binary collisions, is shown as a black dashed line.

with $\kappa = 0.2$ [25].

The pQCD inelastic scattering cross section has been calculated in [26]. This cross section contains 5 matrix elements for gluon emission from the heavy quark and the light quark and gluon, respectively. Also for the inelastic cross section the momentum of the plasma particle is chosen by a Monte Carlo approach from the local thermal distribution. As in the elastic cross section, the gluon propagator is regulated by $m_{\rm eff} = \kappa m_D(T)$. For the gluon emission vertex a constant $\alpha_S = 0.3$ is used. The emitted gluon is considered as massless. The different limits of the pQCD cross section calculations as well as more details of the approach have been discussed in Ref. [26].

The validity of this approach can be confirmed by comparing its spatial diffusion coefficient \mathcal{D}_s [52] with lattice calculations. Fig. 11 shows $2\pi T\mathcal{D}_s$ of our model, in comparison with recent unquenched lattice data [53]. The former lattice data for $2\pi T\mathcal{D}_s$ were calculated in a quenched approximation, so we do not include them here. We see that both coefficients agree well for $\kappa = 0.2$ whereas there are large differences for the choice $\kappa = 1$. Inelastic collisions have only a negligible influence on \mathcal{D}_s .

Both, the elastic as well as the inelastic collisions, have been already employed in the EPOS2 and EPOS3 framework to described heavy meson data in heavy-ion collisions at LHC energies [13, 54]. We use this theoretical framework without modification also in this new EPOS4HQ version. In this paper the K-factor for elastic as well as for inelastic collisions, which has been varied in the past Refs. [13, 54] in calculations in which the HQ part was coupled to EPOS2 or EPOS3, is equal one, so the calculated pQCD cross sections are not modified by

an overall factor.

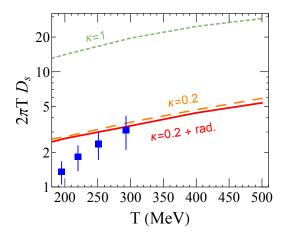


FIG. 11. $2\pi T\mathcal{D}_s$ obtained in our approach in comparison with lattice data from [53]. The plain red line corresponds to our collisional+radiative model (K=1), while the orange long-dashed line represents the contribution from the sole collisional part; the dashed curves illustrates the equivalent calculation if the IR regulator is taken as the Debye mass $(\kappa=1)$.

Fig. 10 displays the change of the momentum distribution of heavy quarks caused by the interactions with the QGP for central PbPb collisions at $\sqrt{s_{\mathrm{NN}}}=5.02$ TeV. As said, the blue line is the initial transverse momentum distribution. The p_T distribution of the heavy quark just before they hadronize is represented by the red line. At low p_T there is little difference between the curves because the initial p_T of the heavy quarks is close to the value one expects if the heavy quarks come to a thermal equilibrium with the light quarks, so the momentum change is small. For large momenta, on the contrary, we observe a p_T shift to lower p_T values of the order of 5 GeV.

V. HADRONIZATION SCHEME

When the QGP has expanded to the critical value of the local temperature or energy density ($T_{\rm FO}=167{\rm MeV}$ or $\epsilon_{\rm FO}=0.57{\rm GeV/fm^3}$), the system hadronizes and the heavy quark converts into a heavy flavor hadron. In the EPOS4HQ framework, there are two ways in which the heavy quark can hadronize, either by fragmentation or by coalescence. In the coalescence process, the heavy quarks coalesce with light quarks from the hypersurface at which they are localized. The fluid at the hypersurface has an average velocity. The momentum of the light quark, with which the parton coalesce, is selected randomly from the thermal distribution with the fluid temperature T_{FO} and the average fluid velocity at the hypersurface.

In this study, we neglect the coordinate information of quarks and require only that the hadronization hypersurface is same for the heavy and light quarks. In the numerical simulation the coalescence formula is applied in the center-of-mass frame of heavy and light quarks.

The momentum distribution of HF hadrons, produced via the coalescence process, can be calculated in the thermal rest system by:

$$\frac{dN}{d^{3}\mathbf{P}} = g_{H} \sum_{N_{Q}} \int \prod_{i=1}^{k} \frac{d^{3}p_{i}}{(2\pi)^{3}} f(\mathbf{p}_{i})$$

$$\times W_{H}(\mathbf{p}_{1}, ..., \mathbf{p}_{i}) \delta^{(3)} \left(\mathbf{P} - \sum_{i=1}^{N} \mathbf{p}_{i}\right), \qquad (1)$$

where g_H is the degeneracy factor of color and spin. **P** and \mathbf{p}_i are the momenta of heavy flavor hadrons and the constituent quarks, respectively. The delta function conserves momentum. The integration is carried at the point where the heavy quark crosses the hadronization hypersurface, which is given by EPOS4. The summation is performed over all heavy quarks in the system. $f(\mathbf{p}_i)$ is the momentum space distribution of the constituent in the heavy hadron at the moment of hadronization with k=2 for mesons and 3 for baryons. $W_H(\mathbf{p}_1,..,\mathbf{p}_k)$ is the Wigner density of a given heavy hadron H, which can be constructed from the heavy hadron wave function, the solution of the Schrödinger equation, and which is approximated here by a three-dimensional harmonic oscillator state with the same root mean square radius. After integration over the coordinate space, the Wigner density of the mesonic ground state can be expressed as

$$W(p_r) = (2\sqrt{\pi}\sigma)^3 e^{-\sigma^2 p_r^2}.$$
 (2)

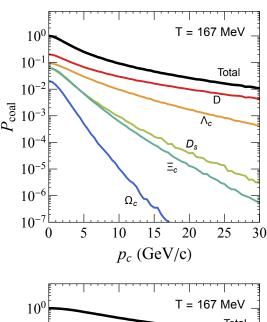
 p_r is the relative momentum between the two constituent quarks in the center-of-mass (CM) frame, $p_r = |E_2\mathbf{p}_1 - E_1\mathbf{p}_2|/(E_1 + E_2)$, $E_1(\mathbf{p}_1)$ and $E_2(\mathbf{p}_2)$ are the energies (momenta) of the quark and antiquark in the heavy hadron CM frame, respectively. Baryons are treated as two two-body systems (baryons are produced by recombining two particles first and then by using their center of mass to recombine this diquark with the third quark).

The light quarks (antiquarks) are assumed to be thermalized. In the rest system of the hypersurface their distribution is given by,

$$f_q(\mathbf{p}_q) = \frac{1}{(2\pi)^3} \frac{g}{e^{E_q/T} + 1},$$
 (3)

where g=6 is the statistical factor. $E_q=\sqrt{\mathbf{p}_q^2+m_q^2}$ is the energy of the light quark. The quark masses are $m_{u/d}=0.1{\rm GeV},\ m_s=0.3{\rm GeV}.$

The heavy quark coalescence probability P_{coal} in a static hot medium with a temperature $T_{\text{FO}} = 167 \text{MeV}$ for the ground states of the open heavy flavor states, e.g. D^0 , D^+ , D_s , Λ_c , Ξ_c , and Ω_c for charm, B^0 , B^- , B_s , Λ_b , Ξ_b , and Ω_b for bottom, is obtained by integrating Eq. (1) with a delta distribution $\delta^3(\mathbf{p}_1 - \mathbf{p}_Q)$ for the momentum of the heavy quark and with a delta distribution $\delta^3(\mathbf{p}_2 - \mathbf{p}_q)$ for the momentum of the quark. p_q is



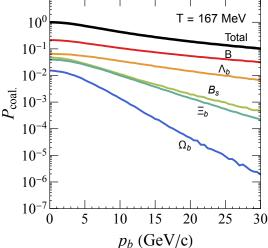


FIG. 12. The momentum dependent coalescence probabilities of charm (upper) and bottom (lower) quark in a hot and static medium with temperature $T=167 {\rm MeV}$.

sampled from the thermal distribution, Eq. (3). We neglect here the rarely produced heavy flavor hadrons, such as multi-charmed (bottomed) baryons, B_c , and quarkonium. For heavy flavor mesons, the averaged square radius can be expressed as $\langle r^2 \rangle = \frac{3}{2} \frac{m_Q^2 + m_q^2}{(m_Q + m_q)^2} \sigma^2$ with charm quark mass $m_c = 1.5 \text{GeV}$ and $m_b = 4.5 \text{GeV}$ for bottom quarks. The root-mean-square radius of the ground state charmed meson has been calculated by the two-body Dirac equation [55]. It gives $\sqrt{\langle r^2 \rangle} = 0.85 \text{fm}$, for in-medium D^0 . So, the corresponding width $\sigma = 3.725 \text{GeV}^{-1}$ for D^0 . In the absence of theoretical studies of the in-medium radius of charmed baryon, we take the same width σ for any two-quark systems in charmed baryons. Because the reduced masses are very similar, the averaged radius of bottom mesons is comparable to that of charmed mesons. So, we take the same width for

TABLE I. Number of excited states considered in EPOS4HQ (N_{excited}) and their relative contributions to the ground states, R_i .

	D^0	D^+	D_s	Λ_c	Ξ_c	Ω_c
$N_{ m excited}$	9	8	5	91	91	53
R	2.91	0.96	2.06	7.63	3.97	4.22
	B^0	B^{-}	B_s	Λ_b	Ξ_b	Ω_b
$N_{ m excited}$	6	6	2	91	91	53
R	2.95	2.95	2.26	7.67	3.92	5.99

bottom mesons and any two-quark systems in bottom baryons.

The coalescence probability of excited states, which can strongly decay into the ground states, is estimated via the statistic model. There the hadron density at the temperature $T_{\rm FO}$ is given by [56],

$$n_i = \frac{g_i}{2\pi^2} T_{\text{FO}} m_i^2 K_2 \left(\frac{m_i}{T_{\text{FO}}}\right), \tag{4}$$

where g_i is the spin isospin degeneracy. m_i is the mass of the hadron. K_2 is the second-order Bessel function. In our study, we consider almost all possible excited states, also the missing baryons, which are predicted by the quark model [57] and lattice QCD [58, 59], as shown in Table I. For each ground state hadron D, D_s , Λ_c , Ξ_c , and Ω_c we calculate the density of their excited states m and define $R^m = n_{\text{excited}}^m / n_{\text{ground}}$. This ratio is momentum-independent. Finally we sum up $R = \sum R^m$ and multiply the ground state momentum-dependent coalescence probability by 1 + R to obtain its effective momentum distribution. The sum of the effective momentum distributions for all hadrons gives the total coalescence probability $P_{\text{coal}}(p)$. Same as for the bottom sector.

The probability that a charm (bottom) quark with a given momentum $\mathbf{p}_c(\mathbf{p}_b)$ forms a specific hadron by coalescence is shown in Fig. 12. Heavy quarks, which do not hadronize via coalescence, will fragment into a heavy-flavor hadron. The fragmentation probability is therefore $1-P_{\text{coal}}$. In EPOS4HQ, we use the heavy quark effective theory-based fragmentation function [50, 60]. The fragmentation ratios to various charmed hadrons are taken as the e^+e^- collisions [61] and are shown in Table II. After the hadronization, all charmed hadrons and light hadrons evolve together in the hadronic phase, which is controlled by the UrQMD [62]. Bottom hadrons do not interact in the hadronic phase.

VI. RESULTS

In this section, we present the EPOS4HQ results for open heavy flavour hadrons. We are as exhaustive as

TABLE II. Fragmentation ratio of charm (bottom) quark to charmed (bottomed) hadrons in percent.

D^{0} 60.8%	D^{+} 24.0%	D_s 8.0%	Λ_c 6.0%	Ξ_c 1.0%	Ω_c 0.2%
B^0 42.4%	B^{-} 42.4%	B_s 8.0%	Λ_b 6.0%	Ξ_b 1.0%	Ω_b 0.2%

possible and show the results for all published experimental data on transverse momentum and elliptic flow. We present as well yield ratios like R_{AA} and interpret these results with help of additional information, which the EPOS4HQ approach provides.

A. Transverse momentum spectra

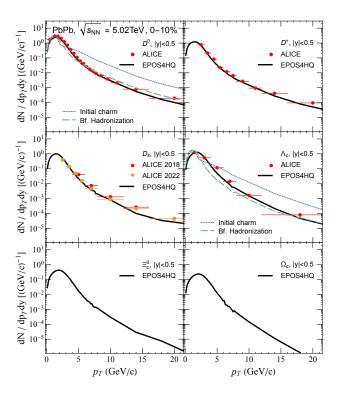


FIG. 13. p_T spectra of charmed hadrons D^0 , D^+ , D_s , Λ_c , Ξ_c^0 , and Ω_c in the 0-10% centrality class of PbPb collisions at $\sqrt{s_{\rm NN}} = 5.02 {\rm TeV}$. The experimental data of D and D^+ [63], D_s [64, 65], Λ_c [66] are from the ALICE. The thick black line is the EPOS4HQ result, the dotted blue and dashed green lines are the p_T distribution of charm quarks at production and before hadronization, respectively, which finally are part of the D^0 (Λ_c).

1. charm hadrons

The transverse momentum spectra of D^0 , D^+ , D_s , Λ_c , Ξ_c , and Ω_c in PbPb collisions at $\sqrt{s_{\rm NN}} = 5.02 {\rm TeV}$ and for 0-10%, 30-50%, and 60-80% centrality are shown in Figs 13 and 14. The EPOS4HQ calculations (thick black line) are compared with the ALICE data: D^0 and D^{+} from [63], D_{s} form [64, 65], and Λ_{c} from [66]. For D^0 (Λ_c) we show as well the initial p_T distribution of those charm quarks which are finally entrained in D^0 (Λ_c) hadrons (dotted blue line) as well as that before hadronization (dashed green line) to demonstrate how the passage through the QGP and the subsequent hadronization modifies the initial distribution. At high transverse momenta the p_T distribution before the cquarks hadronizes is strongly suppressed as compared to the initial distribution, testifying the energy loss of the c-quark in the QGP. At low momentum, when the momentum of the c-quark is of the order of the averaged momentum of the QGP partons, collisions have the consequence that the c-quarks approaches an equilibrium with the QGP. Comparing the dashed green line to the black line, we can see clearly the influence of the hadronization on the transverse momentum change. High p_T charm hadronizes almost exclusively via fragmentation, which shifts the spectra to lower p_T . Low p_T charm hadronizes by combining with another light antiquark (or two light quarks for baryons), which shifts the momentum to a higher region. This momentum shift is more pronounced for Λ_c due to two light quarks entrained. Where data are available the transverse momentum distributions of EPOS4HQ are for all centrality bins close to the measured ones.

The p_T spectra of different charmed hadrons, produced in AuAu collisions at RHIC at $\sqrt{s_{\rm NN}} = 200 {\rm GeV}$ and in the 0-10% and 10-40% centrality bins are shown in Figs. 15. The EPOS4HQ results (thick black line) are compared with the STAR data [67] for D-mesons and [68] for D_s mesons. For the D^0 data we show as well the initial p_T distribution of those charm quarks which are finally entrained in a D^0 meson (dotted blue line) as well as that before hadronization (dashed green line) to demonstrate how the passage through the QGP and the subsequent hadronization modifies the initial distribution. As compared to the LHC results the energy loss while traversing the QGP shifts the momentum less and therefore the spectrum at high p_T is less suppressed. Also at RHIC we reproduce nicely the available experimental data.

2. bottom hadrons

The transverse momentum spectra of bottom hadrons B^0 , B^- , B_s , Λ_b , Ξ_b , and Ω_b in the 0-100% centrality class of PbPb collisions at $\sqrt{s_{\rm NN}} = 5.02 {\rm TeV}$ are shown in Fig. 16. The experimental data of B^0 [69] and B_s [70] are from the CMS collaboration. For the B^0 data we show as well

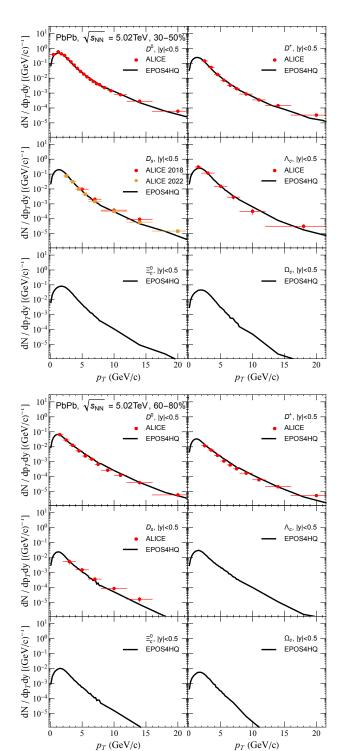


FIG. 14. p_T spectra of charmed hadrons D^0 , D^+ , D_s , Λ_c , Ξ_c^0 , and Ω_c in the 30-50% and 60-80% centrality classes of PbPb collisions at $\sqrt{s_{\rm NN}}=5.02{\rm TeV}$. The experimental data of D and D^+ [64], D_s [64], Λ_c [66] are from the ALICE.

the initial p_T distribution of the charm quarks (dotted blue line) as well as that before hadronization (dashed green line), which are finally part of B^0 mesons. The

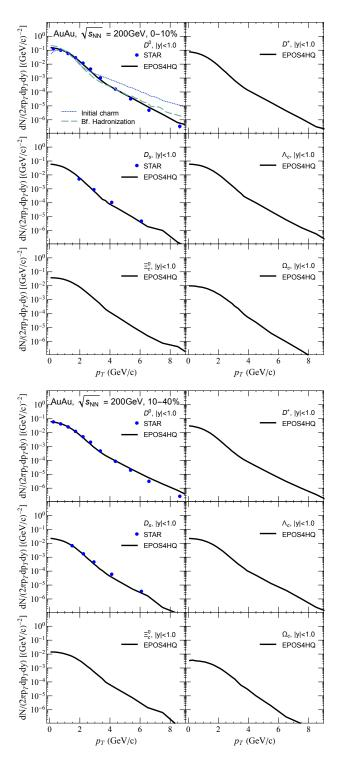


FIG. 15. p_T spectra of charmed hadrons D^0 , D^+ , D_s , Λ_c , Ξ_c^0 , and Ω_c in the 0-10% and 10-40% centrality classes of AuAu collisions at $\sqrt{s_{\rm NN}}=200{\rm GeV}$. The experimental data of D [67], D_s [68] are from the STAR. The thick black line is the EPOS4HQ result, the dotted blue and dashed green lines are the p_T distribution of charm quarks at production and before hadronization, respectively, which finally are entrained in D^0 mesons.

momentum loss of a bottom quark while passing through the plasma is less than that of a charm quark. This is due to the kinematics of the interaction of the large mass b-quarks with the QGP partons, which suppresses the momentum transfer as compared to the interaction of c-quarks.

Another source of information about B-mesons are the decay products, especially the non-prompt J/ψ s. Their p_T spectrum has been measured for central events in PbPb at $\sqrt{s_{\rm NN}} = 5.02$ GeV by the ATLAS [71] and the ALICE [72] collaborations. Their results are displayed in Fig. 17 and compared to that of EPOS4HQ calculations. We display in this figure as well the p_T distribution of the B^0 mesons in this centrality bin. In our calculation we assumed that non-prompt J/ψ come exclusively from B^0 decays and that the experimental p_T differential branching ratio $\mathcal{B}(p_T)$ is the same in pp as in PbPb. Then we can calculate the non-prompt J/ψ p_T spectrum in PbPb by multiplying the calculated $B^0(p_T)$ spectrum in PbPb with $\mathcal{B}(p_T)$. Doing this we assume that shadowing does not influence the branching ratio, an assumption which creates an additional uncertainty.

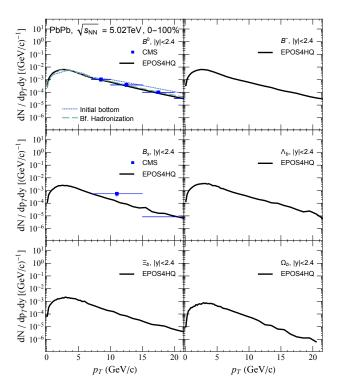


FIG. 16. p_T spectra of charmed hadrons B^0 , B^- , B_s , Λ_b , Ξ_b , and Ω_b in the 0-100% centrality class of PbPb collisions at $\sqrt{s_{\rm NN}}=5.02{\rm TeV}$. The experimental data of B^0 [69] and B_s [70] are from the CMS collaboration. The thick black line is the EPOS4HQ result, the dotted blue and dashed green lines are the p_T distribution of bottom quarks at production and before hadronization, respectively, which finally are entrained in B^0 mesons.

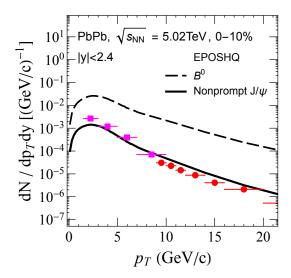


FIG. 17. p_T spectrum of B^0 and nonprompt J/ψ in the 0-10% PbPb collisions at 5.02TeV. The experimental data are from the ATLAS [71] and ALICE [72].

B. Yield ratio

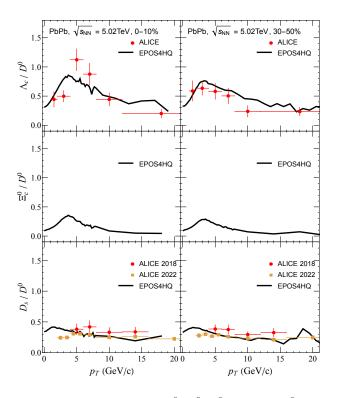


FIG. 18. Yield ratio of Λ_c/D^0 , Ξ_c^0/D^0 , and D_s/D^0 in the 0-10% (left) and 30-50% (right) centrality class of PbPb collisions at $\sqrt{s_{\rm NN}}=5.02{\rm TeV}$. The experimental data are from the ALICE, Λ_c/D^0 [66], D_s/D^0 [64, 65].

Next we present the yield ratio between different heavy flavor hadrons as a function of p_T . Yield ratios of

charmed hadrons are important because they present an experimental probe to study fragmentation functions into the different hadron species. This is especially true at high p_T where on the one side hadrons are almost exclusively produced by fragmentation and on the other side hardly any theoretical calculation of these fragmentation functions is available. Yield ratios can also eliminate systematic uncertainties and have therefore a smaller error than absolute yields. They may also contribute to solve physics questions. For example, the yield ratio of D_s/D^0 can reveal the strangeness enhancement in the QGP phase of the heavy-ion collisions. The enhancement of the baryon to meson ratio, as compared to the e^+e^- collisions, e.g. p/π , Λ/K , shows the importance of hadronization by recombination which is absent in e^+e^- collision where hadronization is exclusively described by fragmentation functions. This enhancement has also been observed in the heavy flavour sector, like in the Λ_c/D^0 ratio, and is even present in high energy pp collisions [66, 73].

In Fig 18 we present the yield ratios of Λ_c/D^0 , Ξ_c^0/D^0 , and D_s/D^0 in the 0-10% (left) and 30-50% (right) centrality classes of PbPb collisions at $\sqrt{s_{\rm NN}} = 5.02 {\rm TeV}$. The experimental data are from the ALICE collaboration, Λ_c/D^0 from [66], D_s/D^0 from [64, 65]. We observe that in both centrality classes the experimental D_s/D^0 ratio is well reproduced by the EPOS4HQ calculations. This is a strong hint that in the QGP, from where the light quarks originate, the strange quark multiplicity corresponds to the equilibrium value for a system close to $T_{\rm FO}$, as assumed in the EPOS4HQ approach. Also the Λ_c/D^0 ratio of EPOS4HQ is for both centrality classes and in the whole p_T interval in agreement with experiment [66], including the peak structure of the distribution at around $p_T = 3$ GeV. This ratio is well above the ratio measured in e^+e^- collisions. The enhancement of the baryon to meson ratio in heavy ion collisions can be well understood within the quark recombination/coalescence model [10, 15, 55, 74, 75] and therefore the agreement between theory and data gives evidence that at low p_T the majority of Λ_c is created in coalescence processes. At higher p_T , where fragmentation dominates, the agreement shows that the employed fragmentation functions [50, 60] are realistic. We also display the prediction for the Ξ_c/D^0 ratio. The shape is similar to the Λ_c/D^0 , but the value is reduced to one half of the former due to the strange quark.

C. Nuclear modification factor R_{AA}

Heavy quarks are produced in primary hard scattering processes, which occur in the early stage of the heavyion collisions. Therefore it is useful to define the nuclear modification factor

$$R_{AA} \equiv \frac{1}{\langle N_{\text{coll}} \rangle} \frac{dN_{AA}/dp_T}{dN_{pp}/dp_T}.$$
 (5)

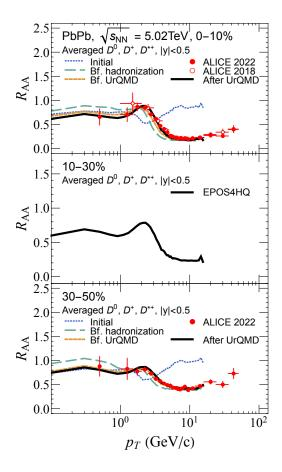


FIG. 19. Nuclear modification factor R_{AA} of D^0 in the 0-10%, 10-30%, and 30-50% PbPb collisions at 5.02TeV. The experimental data are from the ALICE [63, 64]. The black thick (orange lines) lines are the ratio of D^0 in PbPb and pp after (before) UrQMD. The blue dotted and green dashed lines are the ratio of charm quarks at production and before hadronization, respectively, which finally are entrained in D^0 mesons.

which compares the p_T distribution in AA collisions with that in pp collisions multiplied by $\langle N_{\rm coll} \rangle$, the average number of initial hard binary collisions. If the p_T distribution, observed in heavy-ion collisions, is just a superposition of that observed in pp collisions we expect $R_{AA}=1$. In Fig. 19 the full black lines show the R_{AA} for the finally observed hadrons, calculated in the EPOS4HQ approach, and the experimental data [63, 64] are marked as red points. We see that R_{AA} is smaller than 1. This has two reasons:

• Nuclear shadowing modifies the parton distribution function of a nucleus in comparison to that of a proton. In [63] the measured integrated R_{AA} for D^0 mesons (0.689 for the centrality [0-10%] and for |y| < 0.5, what EPOS4HQ reproduces within the error bars) is compared with perturbative QCD calculations of D^0 -meson production including only initial-state effects modeled using two different sets of nuclear parton distribution functions (PDF),

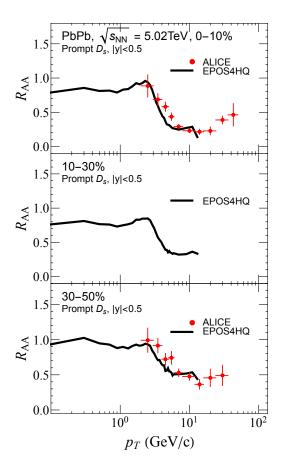


FIG. 20. Nuclear modification factor R_{AA} of D_s in the 0-10%, 10-30%, and 30-50% PbPb collisions at 5.02TeV. The experimental data are from the ALICE [65].

namely nCTEQ15 and EPPS16. These calculations show, however with a large error bar, that the major fraction of the suppression comes from the PDF's, i.e. from the fact that in a nucleus the parton distribution function is different than in a proton. This is confirmed by EPOS4HQ. The R_{AA} for the initially produced charm quarks as around 1 at large p_T but is almost constant ~ 0.7 at low p_T values, as seen in Fig. 19, top, as a blue dotted line. There we display R_{AA} as a function of p_T for [0-10%] central PbPb collisions at $\sqrt{s_{\rm NN}} = 5.02$ TeV. After production, heavy quarks propagate in the QGP and interact with the thermal partons by exchanging energy and momentum via elastic and inelastic collisions, as discussed in section III. Due to the energy loss, at high p_T the initial momentum of a c-quark will shift to a lower momentum, the spectrum becomes softer and R_{AA} falls well below one (green dashed line). At low p_T the momentum of the c-quark increases due to these collisions and the c-quarks approaches thermal equilibrium. This leads to a slight increase of R_{AA} .

• Second, due to hadronization by coalescence, which

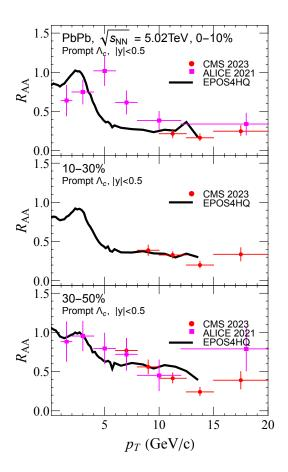


FIG. 21. Nuclear modification factor R_{AA} of Λ_c in the 0-10%, 10-30%, and 30-50% PbPb collisions at 5.02TeV. The experimental data are from the ALICE [66] and CMS [76].

is more important in AA than in pp collisions, we observe at low p_T an increased production of heavy baryons and therefore a lower production of heavy mesons. This lowers R_{AA} at low p_T , as seen, when comparing the green dashed and the orange line.

Both processes lead to a complex structure of R_{AA} with a maximum at intermediate p_T . For less central collisions, shown in Fig. 19 in the middle for [10-30%] and in the bottom row for [30-50%] centrality, the form of R_{AA} as a function of p_T is similar but R_{AA} increases because the energy loss in the plasma gets smaller. The R_{AA} of D_s and Λ_c are also investigated and shown in Figs. 20 and 21, which show a good agreement with the experimental data.

Fig. 22 shows the centrality dependence of R_{AA} for D^0 -mesons in AuAu collisions at $\sqrt{s_{\rm NN}}=200$ GeV. We display $R_{AA}(p_T)$ for two different centrality classes [0-10%] and [10-40%] and for the p_T interval for which experimental data are available and not only extrapolations. The STAR data are from [67]. In this figure we display as well the R_{AA} of the those c-quarks quarks which are later part of D^0 mesons. The blue dotted line shows R_{AA} at the moment when the c-quarks are produced. Also at

RHIC energies for large p_T c-quarks R_{AA} is equal one because shadowing modifies only the c-quark distribution at low p_T . There the suppression of c-quarks in AuAu can reach 50% as compared to pp. The interaction of heavy quarks with the QGP (difference between green long dashed line and the blue dotted line) modifies strongly the R_{AA} at high p_T . Coalescence dominates for low p_T heavy quarks and therefore the momentum of the D-meson is larger than that of the heavy c-quark embedded, leading to an enhancement of R_{AA} at small p_T (difference between dashed orange and long dashed green line). The final hadronic interactions (difference between black and long dashed green line) have little influence of the final form of $R_{AA}(p_T)$.

Finally we compare in Fig. 23 $R_{AA}(p_T)$ of B^+ mesons, measured by the CMS collaboration for PbPb collisions at $\sqrt{s_{\mathrm{NN}}}=5.02$ TeV with the EPOS4HQ calculations. B-mesons are too heavy to approach equilibrium with the QGP. For this reason we observe only a momentum shift of the b-quarks towards lower p_T values. The data agree quite nicely with the EPOS4HQ calculations.

From the confrontation of the EPOS4HQ results with calculations employing the generalized parton distribution function we can conclude that the shadowing in EPOS4HQ is well described. From the agreement of the EPOS4HQ results with data we can furthermore conclude that also the other processes, which influence the final p_T distributions of open heavy flavour mesons, are quite reasonable described.

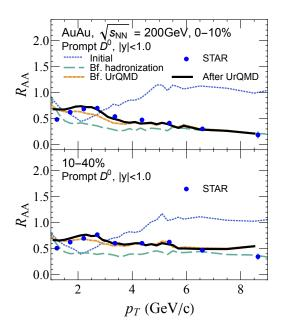


FIG. 22. Nuclear modification factor R_{AA} of D^0 in the 0-10% and 10-40% AuAu collisions at 200GeV. The experimental data are from the STAR [67]. The black thick (orange lines) lines are the ratio of D^0 in AuAu and pp after (before) UrQMD. The blue dotted and green dashed lines are the ratio of charm quarks at production and before hadronization, respectively, which finally are entrained in D^0 mesons.

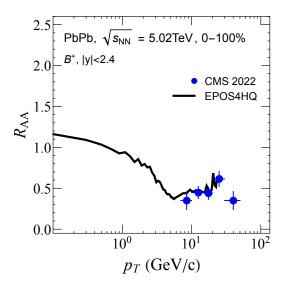


FIG. 23. Nuclear modification factor R_{AA} of B^+ in the 0-100% PbPb collisions at 5.02TeV. The experimental data is from the CMS collaboration [69].

D. Elliptic flow v_2

The elliptic flow v_2 is another key observable to study the interaction of heavy quarks with the QGP. In noncentral heavy ion collisions, the initial spatial anisotropy of the overlap region is converted into an anisotropic azimuthal distribution in momentum space of the final particles at low p_T . This anisotropy can be characterized in terms of Fourier coefficients

$$v_n \equiv \langle \cos[n(\Phi - \Psi_n)] \rangle,$$
 (6)

where Φ is the azimuthal angle of the particle and Ψ_n is the azimuthal angle of the event plane for the nth-order harmonics. Elliptic flow, v_2 , is the second-order coefficient, whose value is in hydrodynamical calculations proportional to the initial spatial eccentricity of the overlap region. Being produced in a hard process, at creation heavy quarks have $v_2 = 0$. So any observed v_2 of heavy mesons is due to the interaction of heavy quarks with QGP partons or of heavy mesons with other hadrons. The final elliptic flow of heavy flavor hadrons comes from the heavy quark itself and also from the light antiquark, which merges with the heavy quark in the hadronization process. Also the hadronization process itself may contribute slightly. The measurement of v_2 of heavy-flavor hadrons at low p_T can therefore help to quantify the coupling between heavy quarks and the hot medium as well as to understand the hadronization mechanism. At high p_T , heavy quarks hadronize via fragmentation. In this case, the elliptic flow v_2 together with R_{AA} can be used to explore the path-length dependence of the in-medium energy loss as in the almond shaped overlap region the

path length of the heavy quark in the QGP medium depends on its azimuthal direction.

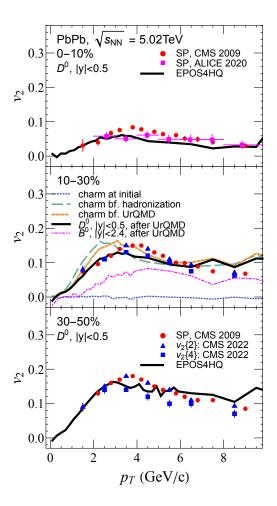


FIG. 24. Elliptic flow v_2 of D^0 in the 0-10%, 10-30%, and 30-50% centrality classes of PbPb collisions at $\sqrt{s_{\rm NN}}=5.02{\rm TeV}$. The experimental data are from the ALICE [77] and CMS [78, 79] collaborations. The black thick (orange lines) lines are the v_2 of D^0 after (before) UrQMD. The blue dotted and green dashed lines are v_2 of charm quarks at production and before hadronization, respectively. The magenta dashed-dotted line in the middle panel is the v_2 of B^0 after UrQMD.

In EPOS4 the event plane Ψ_n can be determined, what is not possible in experiments with a limited acceptance. Therefore a multi particle correlation or cumulants method has been developed to determine v_2 . Depending on the number n of particles, whose correlations are calculated, the result is named $v_2\{n\}$. The higher the order, the more non-flow effects, such as resonance decays and jets, are eliminated. This technique has been widely applied in the light-flavor sector [81]. Recently it has also been used for the heavy flavour flow analysis [79].

In Fig. 24 we show the p_T dependence of $v_2\{2\}$ and $v_2\{4\}$ of D^0 mesons measured by the CMS collaboration [79] at midrapidity for PbPb collisions at $\sqrt{s_{\rm NN}}=5.02$ TeV in different centrality bins. From top to bottom

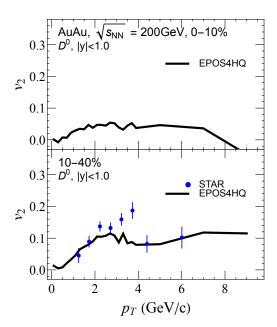


FIG. 25. Elliptic flow v_2 of D^0 in the 0-10% and 10-40% centrality classes of AuAu collisions at $\sqrt{s_{\rm NN}} = 200 {\rm GeV}$. The experimental data are from the STAR [80].

we display the results for the centrality bins [0-10%], [10-30%] and [30-50%]. We see that indeed the experimental $v_2\{4\}$ is slightly smaller than $v_2\{2\}$. In older publications usually $v_2\{2\}$ or the equivalent scalar product (SP) approach has been used. The EPOS4HQ results, obtained with Eq. (6) and shown as well, should be compared with $v_2\{4\}$.

We display in this figure as well the EPOS4HQ results for different times during the evolution of the heavy-ion reaction. Initially the flow of heavy quarks (dotted blue line) is compatible with zero. After passing through the QGP (dashed green line) the c-quarks have acquired already v_2 by collisions with the QGP partons. Hadronization does not change v_2 substantially as can be concluded by comparing the orange short-dashed line (v_2 of D^0 mesons after hadronization) with the green dashed line but shifts the maximum to larger p_T values, mainly because the p_T of the D-meson is different from that of the c-quark. Hadronic interactions (the difference between the orange and the black line) still change slightly the value of $v_2(p_T)$. The final distribution is given by the black line which agrees quite nicely with the experimental data. For the [30-50%] centrality bin we show in Fig. 24 as well v_2 of the B^0 mesons, as a magenta dashed-dotted line, for which no data exists. At low p_T it is considerable smaller than that of the D^0 mesons because due to their large mass the transfer of v_2 to b-quarks during the interactions with the QGP partons is less efficient. At higher p_T , where the v_2 is created by the path length difference, v_2 of B^0 mesons approaches that of D^0 mesons because the mass difference gets increasingly less important.

At RHIC $v_2(p_T)$ of D^0 mesons has been measured by

the STAR collaboration [80]. The data for semicentral AuAu collisions at $\sqrt{s_{\rm NN}}=200$ GeV are displayed in Fig. 25 and compared with EPOS4HQ results. We display in this figure also our results for central collisions for which no data are available yet.

VII. SUMMARY

We used the newly developed EPOS4 approach, which describe quite well a multitude of light hadron observables, to study the physics of heavy quarks. For this we implemented the same description of the dynamics of heavy quarks in the QGP as in the former EPOS3/EPOS2 calculations and included a new hadronization approach, which allows to create in the hadronization process all known heavy hadron species. This approach is named EPOS4HQ. In this approach we investigated the production of heavy hadrons in ultrarelativistic heavy-ion collisions at RHIC and LHC energies. We compared transverse momentum spectra, yield ratio, nuclear modification and elliptic flow of different charmed hadrons for both PbPb collisions at $\sqrt{s_{\mathrm{NN}}}$ = 5.02 TeV and AuAu collisions at $\sqrt{s_{\rm NN}} = 200$ GeV. As already in pp collisions, we find a quite good agreement of all observables with the available experimental data. This agreement is considerable better than for the results we obtained using the same description of the heavy quark/heavy meson dynamics in EPOS2 and EPOS3. We can also extend this approach to RHIC energies what was not possible with the EPOS3/EPOS2 approach.

We studied as well in detail how the different observables are modified during the heavy ion collisions. We displayed the initial distribution of c-quarks, the modification of the c-quark distribution due to heavy quark - QGP interactions, the influence of hadronization and of the final hadronic rescattering. This allowed for an understanding of this physical processes which influence the heavy quark observables. We observed that the initial parton distribution function in large nuclei shows already to a strong suppression of low p_T heavy quarks as compared to the scaled pp parton distribution function. This agrees quantitatively with calculations, which use explicitly generalized parton distribution function. At high p_T , where the parton distribution functions in nucleons and heavy nuclei are similar, the interaction of the heavy quarks with the QGP medium are responsible for the low R_{AA} values. The other processes are subdominant but influence quantitatively the results. The elliptic flow at low p_T is as well created by the interaction of the heavy quarks with the QGP medium but its maximum is shifted in the hadronization process. At high p_T it is the path length difference which creates the finite v_2 values. Despite EPOS4HQ is based on the fundamental Gribov-Regge approach and describes all presently available heavy hadron data in heavy ion collisions it should be noted that EPOS4HQ needs parametrization to cope with kinematic ranges, which are not accessible by more

fundamental approaches. Therefore it cannot be proven whether all the subprocesses are described correctly. The agreement of the EPOS4 results with the light hadron section reduced the uncertainty considerable. An experimental study of the system size dependence would further help to reduce the uncertainties.

Acknowledgement: We thank E. Bratkovskaya and T. Song for fruitful discussions; This work is supported by the European Union's Horizon 2020 research and innovation program under grant agreement No 824093 (STRONG-2020).

- [1] G. Agakishiev et al. (STAR), Phys. Rev. Lett. 108, 072301 (2012), arXiv:1107.2955 [nucl-ex].
- [2] A. Adare et al. (PHENIX), Phys. Rev. Lett. 98, 162301 (2007), arXiv:nucl-ex/0608033.
- [3] V. Khachatryan et al. (CMS), JHEP 04, 039 (2017), arXiv:1611.01664 [nucl-ex].
- [4] T. Matsui and H. Satz, Phys. Lett. B 178, 416 (1986).
- [5] D. Teaney, Phys. Rev. C 68, 034913 (2003), arXiv:nucl-th/0301099.
- [6] P. Kovtun, D. T. Son, and A. O. Starinets, Phys. Rev. Lett. 94, 111601 (2005), arXiv:hep-th/0405231.
- [7] S. Acharya et al. (ALICE), arXiv:2211.04384 [nucl-ex].
- [8] T. Song, H. Berrehrah, D. Cabrera, J. M. Torres-Rincon, L. Tolos, W. Cassing, and E. Bratkovskaya, Phys. Rev. C 92, 014910 (2015), arXiv:1503.03039 [nucl-th].
- [9] T. Song, H. Berrehrah, D. Cabrera, W. Cassing, and E. Bratkovskaya, Phys. Rev. C 93, 034906 (2016), arXiv:1512.00891 [nucl-th].
- [10] S. Plumari, V. Minissale, S. K. Das, G. Coci, and V. Greco, Eur. Phys. J. C 78, 348 (2018), arXiv:1712.00730 [hep-ph].
- [11] F. Scardina, S. K. Das, V. Minissale, S. Plumari, and V. Greco, Phys. Rev. C 96, 044905 (2017), arXiv:1707.05452 [nucl-th].
- [12] V. Minissale, S. Plumari, and V. Greco, Phys. Lett. B 821, 136622 (2021), arXiv:2012.12001 [hep-ph].
- [13] M. Nahrgang, J. Aichelin, S. Bass, P. B. Gossiaux, and K. Werner, Phys. Rev. C 91, 014904 (2015), arXiv:1410.5396 [hep-ph].
- [14] S. Cao, T. Luo, G.-Y. Qin, and X.-N. Wang, Phys. Rev. C 94, 014909 (2016), arXiv:1605.06447 [nucl-th].
- [15] M. He and R. Rapp, Phys. Rev. Lett. 124, 042301 (2020), arXiv:1905.09216 [nucl-th].
- [16] M. He and R. Rapp, Phys. Lett. B 795, 117 (2019), arXiv:1902.08889 [nucl-th].
- [17] S. Cao, G.-Y. Qin, and S. A. Bass, Phys. Rev. C 92, 024907 (2015), arXiv:1505.01413 [nucl-th].
- [18] A. Beraudo, A. De Pace, M. Monteno, M. Nardi, and F. Prino, Eur. Phys. J. C 82, 607 (2022), arXiv:2202.08732 [hep-ph].
- [19] A. Beraudo, A. De Pace, D. Pablos, F. Prino, M. Monteno, and M. Nardi, (2023), arXiv:2306.02152 [hep-ph].
- [20] P. B. Gossiaux, S. Vogel, H. van Hees, J. Aichelin, R. Rapp, M. He, and M. Bluhm, (2011), arXiv:1102.1114 [hep-ph].
- [21] K. Werner, Phys. Rev. C 108, 064903 (2023), arXiv:2301.12517 [hep-ph].
- [22] K. Werner and B. Guiot, Phys. Rev. C 108, 034904 (2023), arXiv:2306.02396 [hep-ph].
- [23] K. Werner, (2023), arXiv:2310.09380 [hep-ph].
- [24] K. Werner, Phys. Rev. C 109, 014910 (2024), arXiv:2306.10277 [hep-ph].
- [25] P. B. Gossiaux and J. Aichelin, Phys. Rev. C 78, 014904

- (2008), arXiv:0802.2525 [hep-ph].
- [26] J. Aichelin, P. B. Gossiaux, and T. Gousset, Phys. Rev. D 89, 074018 (2014), arXiv:1307.5270 [hep-ph].
- [27] V. N. Gribov, Zh. Eksp. Teor. Fiz. 53, 654 (1967).
- [28] V. N. Gribov, Sov. Phys. JETP 29, 483 (1969).
- [29] V. N. Gribov and L. N. Lipatov, Sov. J. Nucl. Phys. 15, 438 (1972).
- [30] V. A. Abramovsky, V. N. Gribov, and O. V. Kancheli, Yad. Fiz. 18, 595 (1973).
- [31] H. J. Drescher, M. Hladik, S. Ostapchenko, T. Pierog, and K. Werner, Phys. Rept. 350, 93 (2001), arXiv:hepph/0007198.
- [32] L. V. Gribov, E. M. Levin, and M. G. Ryskin, Phys. Rept. 100, 1 (1983).
- [33] L. D. McLerran and R. Venugopalan, Phys. Rev. D 49, 2233 (1994), arXiv:hep-ph/9309289.
- [34] L. D. McLerran and R. Venugopalan, Phys. Rev. D 49, 3352 (1994), arXiv:hep-ph/9311205.
- [35] A. Kovner, L. McLerran, and H. Weigert, Phys. Rev. D52, 3809 (1995), hep-ph/9505320.
- [36] Y. V. Kovchegov, Phys. Rev. D54, 5463 (1996), hep-ph/9605446.
- [37] Y. V. Kovchegov and D. H. Rischke, Phys. Rev. C56, 1084 (1997), hep-ph/9704201.
- [38] J. Jalilian-Marian, A. Kovner, L. McLerran, and H. Weigert, Phys. Rev. **D55**, 5414 (1997), hepph/9606337.
- [39] J. Jalilian-Marian, A. Kovner, A. Leonidov, and H. Weigert, Nucl. Phys. **B504**, 415 (1997), hep-ph/9701284.
- [40] Y. V. Kovchegov and A. H. Mueller, Nucl. Phys. B529, 451 (1998), hep-ph/9802440.
- [41] A. Krasnitz and R. Venugopalan, Nucl. Phys. B557, 237 (1999), hep-ph/9809433.
- [42] J. Jalilian-Marian, A. Kovner, A. Leonidov, and H. Weigert, Phys. Rev. **D59**, 034007 (1999), hepph/9807462.
- [43] J. Jalilian-Marian, A. Kovner, and H. Weigert, Phys. Rev. D59, 014015 (1999), hep-ph/9709432.
- [44] V. Khachatryan et al. (CMS), JHEP 09, 091 (2010), arXiv:1009.4122 [hep-ex].
- [45] K. Werner, Phys. Rev. Lett. 98, 152301 (2007), arXiv:0704.1270 [nucl-th].
- [46] K. Werner, I. Karpenko, T. Pierog, M. Bleicher, and K. Mikhailov, Phys. Rev. C 82, 044904 (2010), arXiv:1004.0805 [nucl-th].
- [47] K. Werner, B. Guiot, I. Karpenko, and T. Pierog, Phys. Rev. C 89, 064903 (2014), arXiv:1312.1233 [nucl-th].
- [48] I. Karpenko, P. Huovinen, and M. Bleicher, Computer Physics Communications 185, 3016 (2014), arXiv:1312.4160.
- [49] M. Cacciari, M. Greco, and P. Nason, JHEP 05, 007 (1998), arXiv:hep-ph/9803400.

- [50] M. Cacciari, P. Nason, and R. Vogt, Phys. Rev. Lett. 95, 122001 (2005), arXiv:hep-ph/0502203.
- [51] S. Acharya et al. (ALICE), (2023), arXiv:2308.04877 [hep-ex].
- [52] H. Berrehrah, P. B. Gossiaux, J. Aichelin, W. Cassing, J. M. Torres-Rincon, and E. Bratkovskaya, Phys. Rev. C 90, 051901 (2014), arXiv:1406.5322 [hep-ph].
- [53] L. Altenkort, D. de la Cruz, O. Kaczmarek, R. Larsen, G. D. Moore, S. Mukherjee, P. Petreczky, H.-T. Shu, and S. Stendebach, (2023), arXiv:2311.01525 [hep-lat].
- [54] M. Nahrgang, J. Aichelin, P. B. Gossiaux, and K. Werner, Phys. Rev. C 90, 024907 (2014), arXiv:1305.3823 [hep-ph].
- [55] J. Zhao, S. Shi, N. Xu, and P. Zhuang, (2018), arXiv:1805.10858 [hep-ph].
- [56] A. Andronic, P. Braun-Munzinger, K. Redlich, and J. Stachel, Phys. Lett. B 659, 149 (2008), arXiv:0708.1488 [nucl-th].
- [57] D. Ebert, R. N. Faustov, and V. O. Galkin, Phys. Rev. D 84, 014025 (2011), arXiv:1105.0583 [hep-ph].
- [58] A. Bazavov et al., Phys. Lett. B 737, 210 (2014), arXiv:1404.4043 [hep-lat].
- [59] M. Padmanath, R. G. Edwards, N. Mathur, and M. J. Peardon, PoS LATTICE2014, 084 (2015), arXiv:1410.8791 [hep-lat].
- [60] E. Braaten, K.-m. Cheung, S. Fleming, and T. C. Yuan, Phys. Rev. D 51, 4819 (1995), arXiv:hep-ph/9409316.
- [61] M. Lisovyi, A. Verbytskyi, and O. Zenaiev, Eur. Phys. J. C 76, 397 (2016), arXiv:1509.01061 [hep-ex].
- [62] S. A. Bass et al., Prog. Part. Nucl. Phys. 41, 255 (1998), arXiv:nucl-th/9803035.
- [63] S. Acharya et al. (ALICE), JHEP 01, 174 (2022), arXiv:2110.09420 [nucl-ex].
- [64] S. Acharya et al. (ALICE), JHEP 10, 174 (2018), arXiv:1804.09083 [nucl-ex].
- [65] S. Acharya et al. (ALICE), Phys. Lett. B 827, 136986

- (2022), arXiv:2110.10006 [nucl-ex].
- [66] S. Acharya et al. (ALICE), Phys. Lett. B 839, 137796 (2023), arXiv:2112.08156 [nucl-ex].
- [67] J. Adam et al. (STAR), Phys. Rev. C 99, 034908 (2019), arXiv:1812.10224 [nucl-ex].
- [68] J. Adam et al. (STAR), Phys. Rev. Lett. 127, 092301 (2021), arXiv:2101.11793 [hep-ex].
- [69] A. M. Sirunyan et al. (CMS), Phys. Rev. Lett. 119, 152301 (2017), arXiv:1705.04727 [hep-ex].
- [70] A. M. Sirunyan et al. (CMS), Phys. Lett. B 796, 168 (2019), arXiv:1810.03022 [hep-ex].
- [71] M. Aaboud et al. (ATLAS), Eur. Phys. J. C 78, 762 (2018), arXiv:1805.04077 [nucl-ex].
- [72] S. Acharya et al. (ALICE), (2023), arXiv:2308.16125 [nucl-ex].
- [73] J. Adam et al. (STAR), Phys. Rev. Lett. 124, 172301 (2020), arXiv:1910.14628 [nucl-ex].
- [74] Y. Oh, C. M. Ko, S. H. Lee, and S. Yasui, Phys. Rev. C 79, 044905 (2009), arXiv:0901.1382 [nucl-th].
- [75] S. Cao, K.-J. Sun, S.-Q. Li, S. Y. F. Liu, W.-J. Xing, G.-Y. Qin, and C. M. Ko, Phys. Lett. B 807, 135561 (2020), arXiv:1911.00456 [nucl-th].
- [76] A. Tumasyan et al. (CMS), (2023), arXiv:2307.11186 [nucl-ex].
- [77] S. Acharya et al. (ALICE), Phys. Lett. B 813, 136054 (2021), arXiv:2005.11131 [nucl-ex].
- [78] A. M. Sirunyan et al. (CMS), Phys. Lett. B 816, 136253 (2021), arXiv:2009.12628 [hep-ex].
- [79] A. Tumasyan et al. (CMS), Phys. Rev. Lett. 129, 022001 (2022), arXiv:2112.12236 [hep-ex].
- [80] L. Adamczyk et al. (STAR), Phys. Rev. Lett. 118, 212301 (2017), arXiv:1701.06060 [nucl-ex].
- [81] S. Chatrchyan et al. (CMS), Phys. Rev. C 87, 014902 (2013), arXiv:1204.1409 [nucl-ex].